

# Oil slicks in the Gulf of Guinea - 10 years of Envisat ASAR observations

Zhour Najoui <sup>a</sup>, Nellya Amoussou <sup>c</sup>, Serge Riazanoff <sup>a,b</sup>, Guillaume Aurel <sup>a</sup>, Frédéric Frappart <sup>d</sup>

<sup>a</sup> VisioTerra, 14 rue Albert Einstein Champs-sur-Marne, France, zhour.najoui-nafai@visioterra.fr, serge.riazanoff@visioterra.fr, guillaume.aurel@visioterra.fr.

<sup>b</sup> Université Gustave Eiffel – Institut Gaspard Monge -IGM, 5 boulevard Descartes, Champs sur Marne, [France](#), serge.riazanoff@visioterra.fr.

<sup>c</sup> Sorbonne Université - Laboratoire d'Océanographie et du Climat : Expérimentations et Approches Numériques (LOCEAN), 4 Place Jussieu, 75005 Paris, [France](#), lydieamoussou14@gmail.com.

<sup>d</sup> INRAE, ISPA, UMR 1391 INRAE/Bordeaux Sciences Agro, Villenave d'Ornon, France, frederic.frappart@inrae.fr.

---

Correspondence to: Zhour NAJOU (zhour.najoui-nafai@visioterra.fr)

---

## 1. Abstract

The Gulf of Guinea is a very active area regarding maritime traffic as well as oil and gas exploitation. Due to some actors failure to comply with environmental standards, this region has been subject to a large number of oil pollution. This pollution comes in addition to natural oil seepages from the ocean floor. This study aims to detect oil slicks spilled in the Gulf of Guinea and analyse their spatial distribution using Synthetic Aperture Radar (SAR) images. The previous works have already locally mapped oil slicks in this area, this study proves to be the first one to achieve a global statistical analysis based on 10 years of radar images covering 17 Exclusive Economic Zones of the Gulf of Guinea. The present study has been based on a database of 3,644 SAR images, collected between 2002 and 2012 by the Advanced SAR (ASAR) sensor onboard the European Spatial Agency (ESA) Envisat mission, which allowed the identification of 18,063 oil slicks. These "Oil slicks" herein detected encompass: - "oil spills" of anthropogenic origin and - "oil seeps" of natural origin (natural oil reservoir leaks).

---

## 2. Introduction

The Deep Water Horizon (DWH) disaster that occurred on April 20, 2010 in the Gulf of Mexico aroused worldwide outrage both for its human and environmental impacts (Leifer et al., 2012). There was great interest of the public, media, politicians and scientists characterized by a meticulous follow-up of the progression of the oil slicks (Caruso et al., 2013; Pinkston and Flemings, 2019). And yet, a disaster similar to that of the DWH would not be surprising along the African coast and, in particular, in the Gulf of Guinea, where recurrent oil spills are observed. These may be caused by deballasting operations (Albakjaji, 2010) and releases due to shipwrecks (Fuhrer, 2012).

If oil constitutes an important resource for the countries of the Gulf of Guinea from an economic point of view (Ovadia, 2016), the environmental impact caused by the frequent oil spills has provoked serious negative effects on both the environment and the local economy (Jafarzadeh et al., 2021; Okafor-Yarwood, 2018; Yagmour et al., 2022). The weakness of national monitoring and legislation control is likely to limit the compliance to the major standards followed by large companies. Thus, the provision of observation tools that can enable people of Africa to ensure good monitoring and better management of the Gulf of Guinea is necessary. This facility is to enable African

31 countries to monitor offshore oil exploitation concessions using free data provided by ESA and now the European Union (EU) in the  
32 framework of the Copernicus programme.

33 Synthetic Aperture Radar (SAR) images have proven to be a useful tool for oil slicks mapping due to the dampening effect that oil has  
34 on capillary and small gravity waves, called Bragg waves. The latter are generated on water by local winds and they are responsible for the  
35 radar backscattering (Gade et al., 1998; Jackson et al., 2004; Mercier and Girard-Arduin, 2006; Shu et al., 2010; Xu et al., 2015). As a  
36 consequence, oil slicks appear darker compared to nearby undampened water surface where Bragg waves produce brighter radar  
37 backscattering. In addition, long-term time-series of radar images are freely available since 1991 (ERS-1 mission was launched in 1991,  
38 ERS-2 in 1995, Envisat in 2002, Sentinel-1a in 2014 and Sentinel-1b in 2016) while near real time radar images are foreseen to be freely  
39 available at least until 2030 owing to Sentinel constellation. This data availability allows extensive studies of past and future pollution as  
40 well as operational detection of oil slicks using satellite radar imagery (Kubat et al., 1998).

41 In this study, SAR images acquired by the European Spatial Agency (ESA) mission Envisat has been used. Envisat was launched on  
42 March 1, 2002, its payload contained ten instruments. The Advanced Synthetic Aperture Radar (ASAR) sensor onboard is the second  
43 generation of SAR instrument developed by ESA, (Louet and Bruzzi, 1999). Envisat nominal life (5 years) has been doubled until the loss of  
44 the satellite on April 8, 2012 (10 years).

45 The Gulf of Guinea is now one of the largest oil producing regions of the world and yet, very few studies have really analysed its  
46 situation regarding oil slicks (both spills and seeps). The present study focuses on the spatial distribution of the oil slicks occurring from  
47 2002 to 2012 by Exclusive Economic Zone (EEZ) throughout the Gulf of Guinea using Envisat ASAR radar images.

---

### 48 3. Presentation of the study area

#### 49 **3.1. Geographic location**

50 The radar images used in this study were acquired over the Gulf of Guinea. This region is located in the Atlantic Ocean in the southwest  
51 of Africa. According to the International Hydrographic Organization (Bassou, 2016), it extends from Guinea Bissau to Angola and covers the  
52 EEZ of 16 countries bordering the coast (extending over 7000 km): Guinea Bissau (GNB), Guinea Conakry (GIN), Sierra Leone (SLE),  
53 Liberia (LBR), Ivory Coast (CIV), Ghana (GHA), Togo (TGO), Benin (BEN), Nigeria (NGA), Cameroon (CMR), Equatorial Guinea (GNQ),  
54 Sao Tome and Principe (STP), Gabon (GAB), Republic of Congo (COG), Democratic Republic of Congo (COD), and Angola (AGO)  
55 (fig. 1).

Code de champ modifié

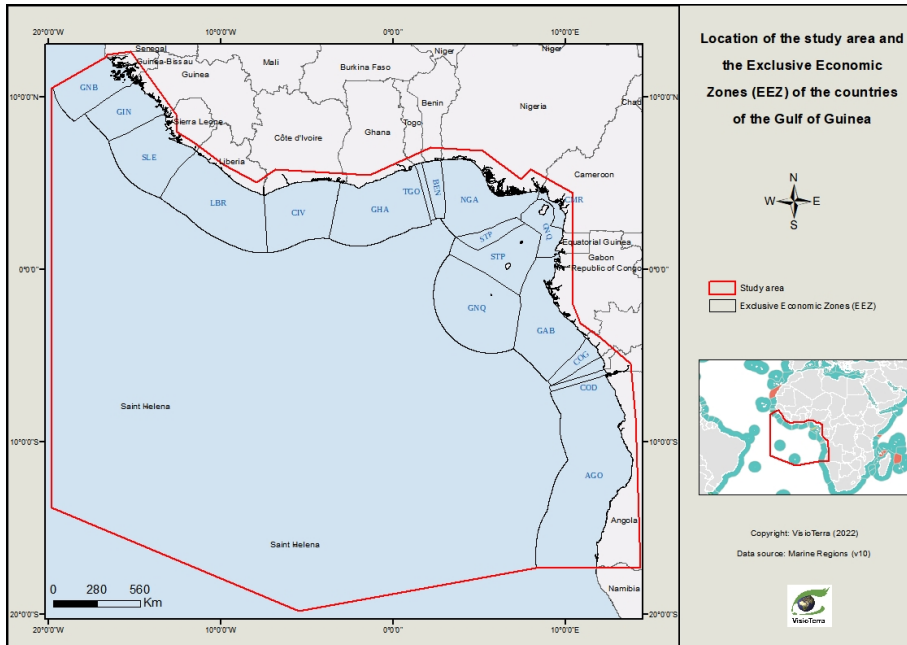


fig. 1 - Location of the study area in the Gulf of Guinea and the Exclusive Economic Zones of the different countries.

### 3.2. Geological location

Petroleum is a natural mixture composed mainly of hydrocarbons. It is formed within certain sedimentary rocks by transformation of organic matter (plankton, plants, animals, etc.) incorporated into the deposit. It is a slow and gradual process occurring in a sedimentary basin.

Indeed, the transformation of organic matter into oil spans millions of years, and has been punctuated by several stages including the formation of an intermediate substance called kerogen. A given layer of sediment sinks and is buried under other layers of sediment. Depending on the filling of the basin, the heat flow and pressure induced by geologic processes, organic matter may change from kerogen to petroleum. Oil being less dense than water, it tends to migrate to the upper layers of the sedimentary strata. These sedimentary strata have a certain geometric configuration defined by the tectonic structure of the basin. During this structuring, different areas may have risen higher (anticlines) or have sunk lower (synclines) relatively to the rest of the stratum. When these upper zones are topped by a cover allowing the oil to escape through faults or fractures, they constitute oil deposits exploited nowadays in offshore or onshore areas.

The Gulf of Guinea is located in a passive zone resulting from the opening of the South Atlantic Ocean initiated during the Lower Cretaceous, breaking up south-west Gondwana. The climate during this period was hot, humid and stable, which favours chemical weathering of the mainland. Eroded material brought chemical elements to the Gulf of Guinea; in particular, the Niger Delta transported sediments rich in hydrocarbons. These numerous characteristics make this area a source of natural seepages also called oil seeps (Lawrence et al., 2002)

### 74 3.3. Oil exploration in the Gulf of Guinea

75 The Gulf of Guinea region has entered the global oil landscape comparatively quite recently. In 1982, the signing of the Montego Bay  
76 convention extended the maritime territories of riparian countries over their EEZ, 200 nautical miles ( $\approx 370$  km) off their coasts, which  
77 encouraged offshore exploration (Bassou 2016). The Gulf of Guinea is now one of the largest oil producing regions in the world.

78 Indeed, since the installation of its first oil platforms (anchored and floating platforms) between 1960 and 1970 (Favenec et al., 2003),  
79 the Gulf of Guinea has become one of the favourite destinations of international oil investors (Tull, 2008). The good quality of its oil justifies  
80 the ~~attractiveness-attraction~~ of foreign countries to the region (Ngodi, 2005). Since the 2000s, it has supplied more than 55 billion barrels, i.e.  
81 5% of world oil production (Mfewou et al., 2018) and 60% of total daily crude oil production in sub-Saharan Africa. Offshore is the default  
82 mode of oil extraction in the Gulf of Guinea (Favenec et al., 2003). The depletion of coastal water resources (shallow water;  $\leq 200$  m)  
83 means that the relative share of deep water exploration (Deep water; 450 m - 1800 m), or even in ultra-deep water (1800 m - 3000 m) is  
84 increasing. This is the case, for example, off the coast of Angola or Gabon.

### 85 3.4. Oil pollution and environmental impacts

86 The Gulf of Guinea is a very active area in oil exploration. The oil spills found in the region are unparalleled in frequency and their  
87 toxicity induces serious repercussions both on the marine environment and on the ecosystem (Bagby et al., 2017; Chalghmi, 2015; Khanna et  
88 al., 2018; Langangen et al., 2017; Li et al., 2019; Li and Johnson, 2019; NAE-NRC, 2012; Reuscher et al., 2020).

89 Several cases of accidents caused by the exploitation of offshore oil are documented. Apart from that, several accidents have occurred  
90 following the exploitation of offshore oil fields. The frequency of oil spills in the Gulf of Guinea is said to be due, among other factors to oil  
91 production operations, inadequate production equipment leading to corrosion of pipelines and tanks, to disasters, sabotage and vandalism  
92 (Adelana and Adeosun, 2011).

93 Environmental consequences include the loss of habitat for corals and seagrass, the destruction of flora (reduction of mangroves and  
94 certain species of algae) and that fauna (extinction of sea turtles) (Scheren et al., 2002). Oil slicks have a devastating effect on fishing  
95 activity. Many Nigerian fishermen can no longer practice their profession, especially off the Niger Delta.

---

## 96 4. Dataset and Method

### 97 4.1. Radar data

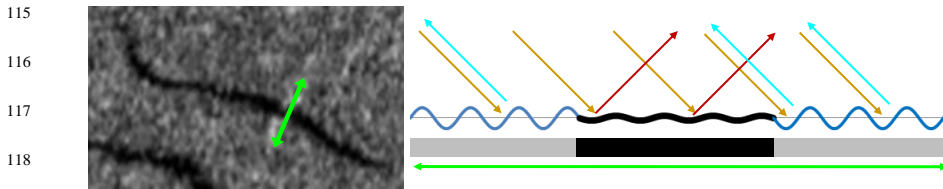
98 Several spaceborne SAR systems have been widely used for marine pollution monitoring and mapping (Brekke and Solberg, 2008; Del  
99 Frate et al., 2000; Dong et al., 2022; Espedal, 1999; Fiscella et al., 2000; Gade et al., 1998; Garcia-Pineda et al., 2008; Kanaa et al., 2003; Li  
100 and Johnson, 2019; Liu et al., 1997; Marghany, 2015; Solberg et al., 1999; Suresh et al., 2015). In this study, we used SAR images acquired  
101 by Envisat ASAR from 2002 to 2012. Envisat ASAR operated at the radar frequency of 5.331 GHz in C-Band (4.20 – 5.75 GHz) in various  
102 modes including WSM (Wide Swath Medium-resolution). WSM ASAR images were acquired along swaths 400 km wide at a spatial  
103 resolution of approximately 150 m by 150 m. WSM products are delivered with a ground pixel spacing of 75 m by 75 m. Envisat ASAR  
104 operated in one of two polarizations types, either HH (horizontal transmission / horizontal reception) or VV (vertical transmission / vertical  
105 reception). ASAR WSM operated according to the ScanSAR principle, using five predetermined overlapping antenna beams (also called sub-

Code de champ modifié

Code de champ modifié

106 swaths) which covered the wide swath. The ScanSAR principle consists in achieving swath widening by the use of an antenna beam which is  
 107 electronically steerable in elevation (Miranda et al., 2013).

108 On a radar image, the areas covered by oil appear as smooth dark regions with low backscattering. This is due to the damping effect that  
 109 the oil produces on capillary waves and small waves of gravity. On a oil-free surface, a significant part of the energy will be backscattered  
 110 towards the radar making it appear lighter (Alpers et al., 2017). The backscatter of the radar signal is also influenced by environmental  
 111 conditions such as: wind speed and sea state (Fingas and Brown, 2017; Zhang et al., 2014). The ideal wind speed for the detection of oil  
 112 slicks is in an interval that depends on the authors: - 2 m/s to 10 m/s (MacDonald et al., 2015), -1.5 m/s to 6.5 m/s (Jatiaux et al.,  
 113 2017), -2.09 m/s to 8.33 m/s (Najoui, 2017)... Vertical polarization (VV) is the most effective mode for detecting oil spills on the sea surface  
 114 (Brekke and Solberg, 2008; Jatiaux et al., 2017; Najoui et al., 2018a, 2018b).



120 *fig. 2 - Backscattering of the radar signal in the presence and absence of oil (Najoui, 2017).*

121 All the Envisat ASAR WSM scenes available in the study area have been processed leading to an amount of **3,644** scenes after  
 122 eliminating redundant products. The fig. 3 illustrates the spatial distribution of the occurrences of Envisat ASAR WSM observations between  
 123 2002 and 2012 in the Gulf of Guinea. The number of WSM observations is noticeably higher near the coasts.

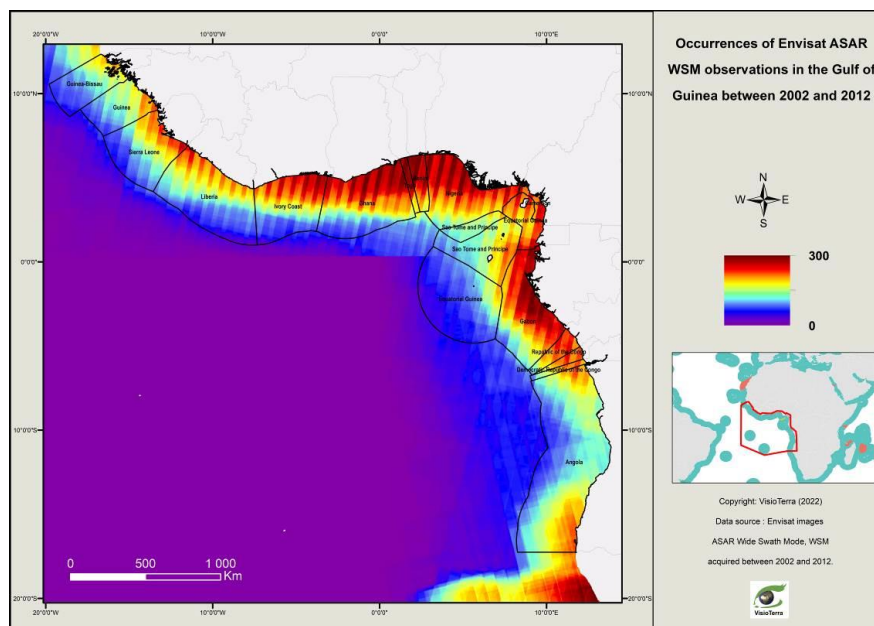


fig. 3 - Occurrences of Envisat ASAR WSM observations between 2002 and 2012.

#### 4.2. Image preprocessing

The database of 3,644 images has been georeferenced in the geographic coordinate reference system over the WGS84 ellipsoid, datum WGS84. A land mask has been applied and the images have been radiometrically corrected. The radiometric correction consists in correcting the brightness variations due to SAR peculiarities. Indeed, the radar backscattering on the offshore area is dominated by non-Lambertian reflections (the surface does not reflect the radiation uniformly in all directions). This non-Lambertian reflection leads to heterogeneity of the brightness in the radar image: brighter along the near-range (closest to the NADIR line) and darker along the far-range. The input images have a 16-bits Digital Number (DN) dynamic which requires reduction to 8-bits to be displayable on a usual screen. The applied preprocessing consists in applying a local stretching with an average of 140 and a standard deviation of 60 on a sliding window of 301 pixels in order to optimize the detectability of the oil slicks (fig. 4) (Najoui, 2017; Najoui et al., 2018b).

135  
136  
137  
138  
139  
140  
141  
142  
143  
144  
145  
146  
147  
148  
149  
150

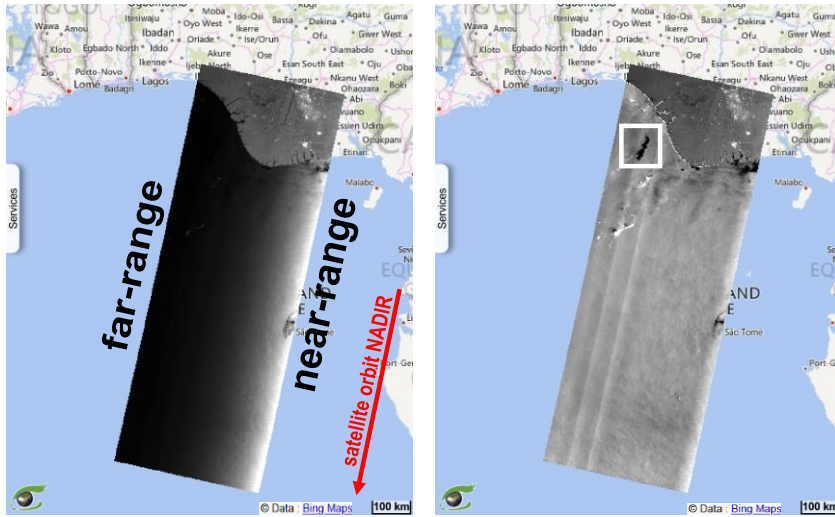
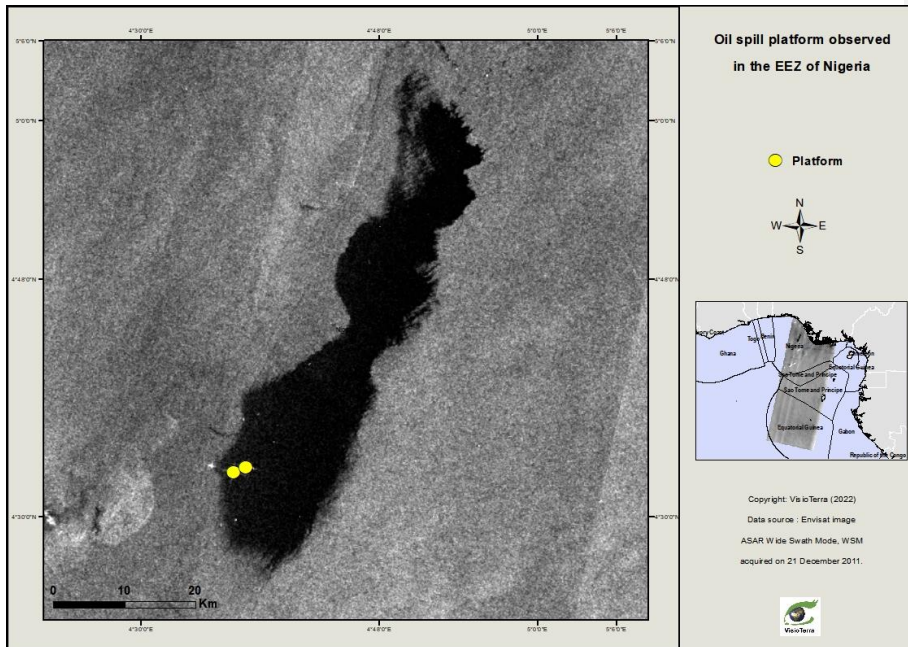


fig. 4 - ASAR WSM images (21/12/2011) before (left) and after (right) local stretching showing a leak from an oil platform (see fig. 5).



151  
152  
153

fig. 5 - Oil spill from platform observed in the EEZ of Nigeria (21/12/2011). The platforms are represented by the yellow dots (see hyperlook <http://visioterra.org/VtWeb/hyperlook/504c7208cc184c12b42ed036bc9912f3>).

#### 154 4.3. Manual detection

155 Oil slicks appear as dark patches on radar images because they flatten the surface of the sea. However, in addition to oil slicks, many  
 156 phenomena also may appear as dark (fig. 6). Non-oil dark patches are termed as look-alikes features that include upwelling, eddies, rainfalls,  
 157 wind shadows, internal waves, etc. (Brekke and Solberg, 2005; Espedal, 1999; Najoui et al., 2018b; Xu et al., 2015). These non-oil features  
 158 are mostly due to meteorological conditions.

159 The detection of oil slicks has been performed using a reliable manual detection approach as explained in Najoui et al. (2018b) and  
 160 Jackson et al. (2004) (Najoui et al., 2018b) (Najoui et al., 2018a; Jackson et al., 2004). In fact, the 3,644 radar images used in this publication  
 161 have been manually interpreted. The detection of oil slicks and their categorisation were carried out following three stages of analysis: 1)  
 162 interpretation based on morphological and textural criteria, 2) multi-date analysis of repetitive oil slicks, and 3) validation using auxiliary  
 163 data.

164 According to the morphological and textural criteria oil slicks may be subdivided into two major classes: biogenic and mineral. Biogenic  
 165 oil slicks are organic films made of substances produced by plankton and other marine organisms. The mineral oil slicks can be subdivided  
 166 between natural seeps (fig. 7), emitted naturally from the sea bottom, and anthropogenic oil spills that originate from ships (fig. 8), refineries,  
 167 oil terminals, industrial plants, oil platforms (fig. 9) and pipelines (Espedal, 1999). If biogenic oil slicks appear as shiny diffracting points on  
 168 radar data, oil seeps are characterized by curvilinear shapes due to short-term changes of the strength and orientation of the wind and of the  
 169 surface currents (Espedal, 1999).

170 For instance, oil spills from platforms or ships induce significant slicks (Johannessen et al., 2000; Leifer et al., 2012; Trivero and  
 171 Biamino, 2010). Oil spills from platforms are characterized by an irregular geometric shape. They may reach large extents and have the  
 172 particularity of being repeated over time. The most distinctive feature is their proximity to oil platforms.-Oil spills from ships have a fine and  
 173 linear geometric shape that may be continuous or intermittent when boats are moving. When the ship is immobile, the oil slick has an  
 174 irregular geometric shape that can be confused with an oil spill from platform. The fig. 6 shows some examples of oil and non-oil patches  
 175 visible in radar images.

176 If biogenic oil slicks appear as shiny diffracting points on SAR data, oil seeps are characterized by curvilinear shapes due to short-term  
 177 changes of the strength and orientation of the wind and of the surface currents (Espedal, 1999).

178 Thereafter, a multi-date analysis has been performed. We use all the interpretations at different dates in order to assess the manual  
 179 interpretation. Indeed, repetitive slicks are, more likely, due to leaks from static sources: a geological feature for oil seeps, a platform or  
 180 pipeline for oil spills, for instance. The shape of these oil slicks from static sources is induced by the strength and orientation of the short-  
 181 term changes of both wind and sea surface current. Usually, this type of slicks from natural oil seeps and oil spills from oil platforms  
 182 constitutes forms of "astroseeps" or "flower structures" (fig. 10). In general, ships that discharge oily effluents do it ~~in-on~~ route, leaving  
 183 behind them linear-shaped spills or trails. When oil is discharged in a current-free and calm sea, the resulting overall spill geometry will  
 184 follow the route of the ship. This linearity is used to identify such oil spills. However, when a deballasting ship maneuvers or when a non-  
 185 uniform surface current is present, then, the contour of the spill can deviate significantly from linearity. When oil is discharged from a  
 186 moving ship, it also spreads laterally, resulting in oil trail which width increases with distance from the ship. In many cases, a white dot  
 187 ahead of the deballasting testifies to the metal structure of the ship and the size, or even the shape, of the dot can be an indicator of the size of  
 188 the vessel.

Mis en forme : Français (France)

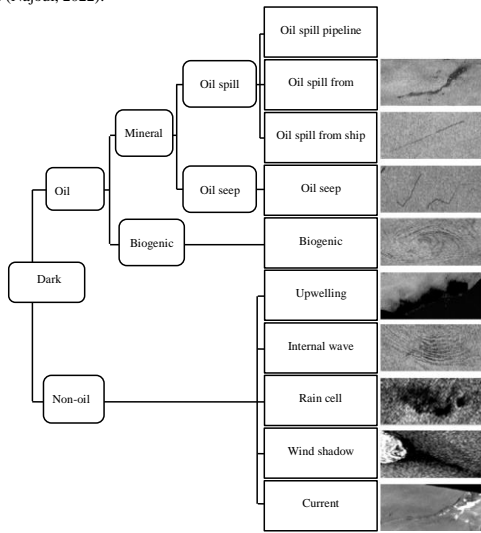
Code de champ modifié

Mis en forme : Français (France)

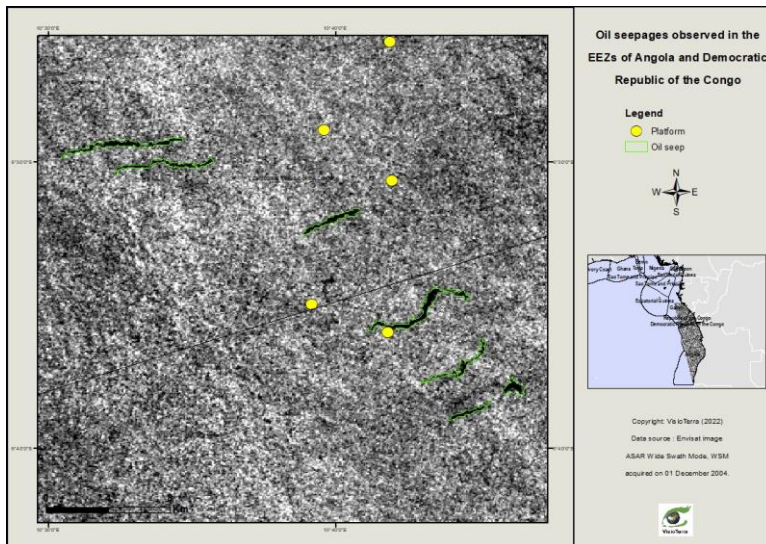
Mis en forme : Anglais (Royaume-Uni)

Mis en forme : Anglais (États-Unis)

189 Finally, the validation of the analysis has been performed by the integration of the manual detection output in a Geographic Information  
 190 System (GIS) with other auxiliary data. These auxiliary data include the location of oil platforms, oil and gas fields, available bathymetric,  
 191 geological and structural data, marine traffic, wind and current field direction... This work has led to ~~the constitution of a~~ dataset with 18,063  
 192 interpreted oil slicks (Najoui, 2022).



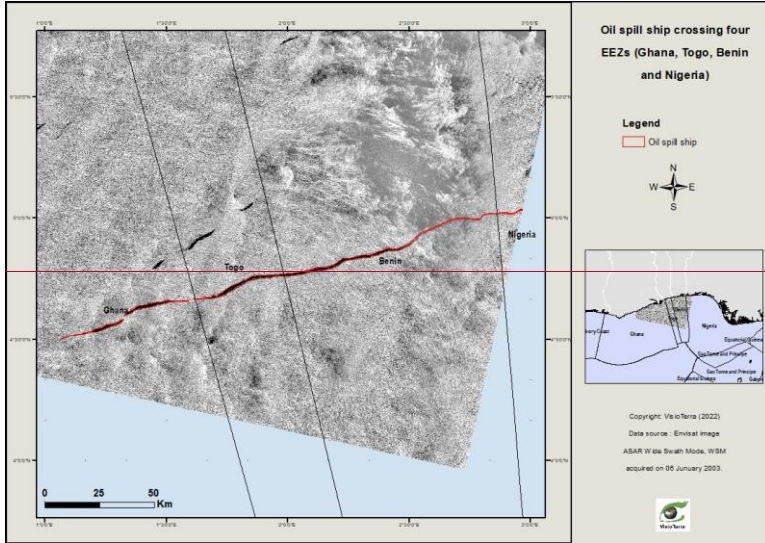
193  
194  
195  
196  
197  
198  
199  
200  
201  
202  
203  
204 *fig. 6 - Main offshore dark patches seen in SAR images (Najoui et al., 2018b)*



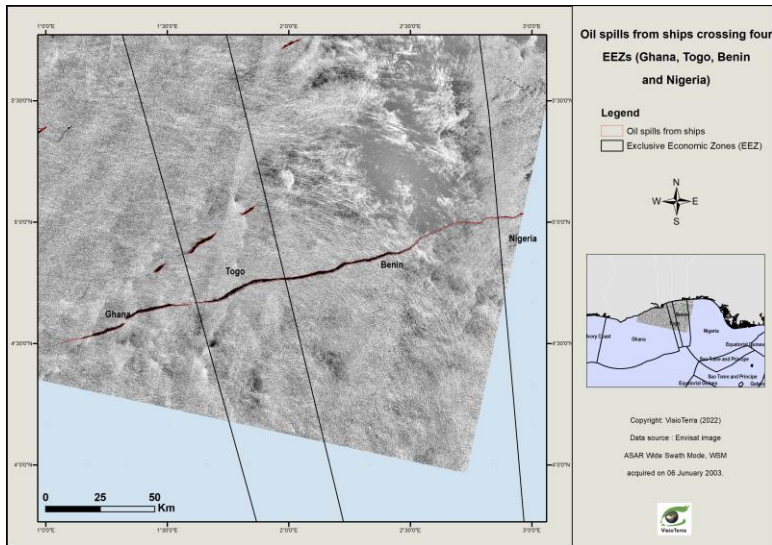
205  
206 *fig. 7 - Oil seeps (1<sup>st</sup> December 2004) observed in the EEZ of Angola and Democratic Republic of the Congo. The*  
 207 *platforms are represented by the yellow dots.*

Mis en forme : Légende figure

Mis en forme : Couleur de police : Noir



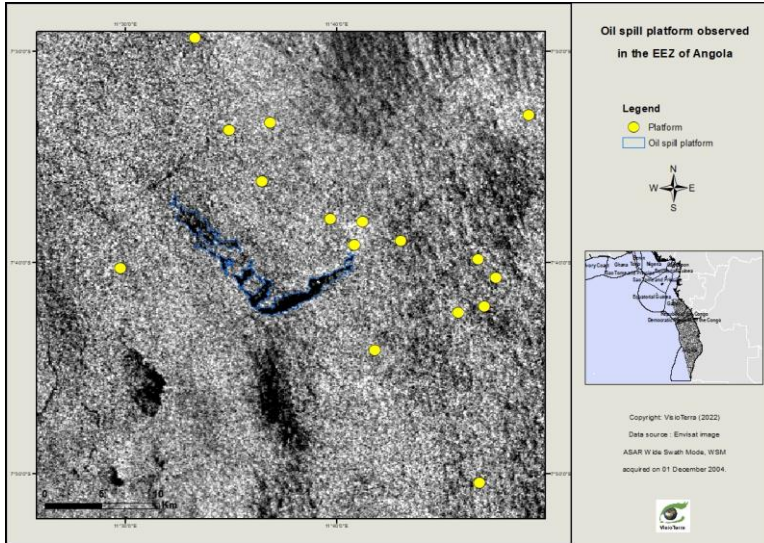
208



209

210

fig. 7fig. 8. - Oil spills from ships (5 January 2003) crossing four EEZs (Ghana, Togo, Benin and Nigeria).

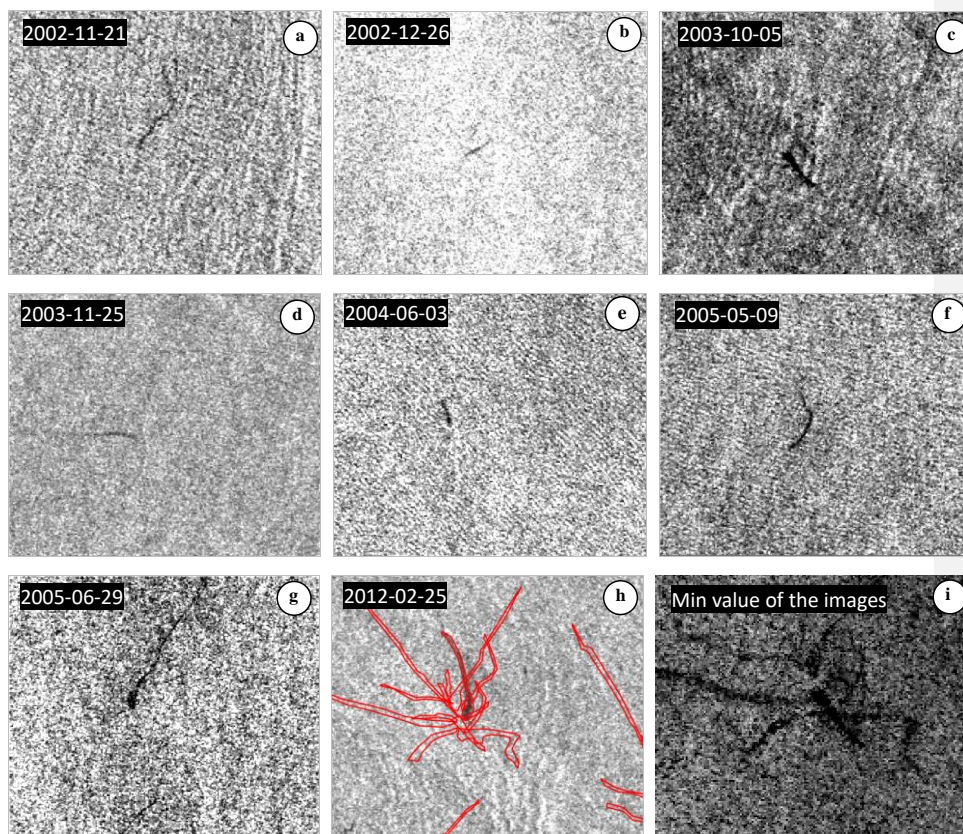


211

212

213

*fig. 8* fig. 9 - Oil spill *from* platform (1<sup>st</sup> December 2004) observed in the EEZ of Angola. The platforms are represented by the yellow dots.



214

215

216

217 *fig. 9* **fig. 10** - Example of multitemporal analysis with astroseeps structure observed in the Lower Congo basin. Images a, b, c, d, e, f and g  
 218 are Envisat ASAR images acquired at different dates with observed seeps. Image h shows an Envisat ASAR image with interpreted seeps.  
 219 Image i shows the Envisat ASAR minimum image (i.e. each pixel is the minimum observed for the 7 dates) with an "astroseep" structure.

#### 220 4.4. Mean area covered in oil

221 The image-interpretation described in the previous section results in the delimitation of closed polygons corresponding to the oil slicks.  
 222 These polygons are "embedded" in a raster image to perform the statistical study. Since each location within the area of interest has not been  
 223 observed an equal number of times by the Envisat satellite, an "observation occurrence map" has been produced (fig. 3). In fact, each  
 224 location has not been equally observed because of the partial overlap of neighbouring swaths and the use of both ascending and descending  
 225 orbits. Hence, it was necessary to locally normalize the oil slicks number distribution by dividing the number of oil slick occurrences by the  
 226 number of observations made by Envisat ASAR over the study area which gives the relative frequency of the presence of oil per pixel.

227 The **probability of presence of oil X per pixel** ( $P_X(l,p)$ ) is equal to the number of occurrences of oil X in a pixel ( $S_X(l,p)$ ) divided by the  
 228 number of observations ( $O(l,p)$ ) of the same pixel (eq.1).

$$P_X(l, p) = \frac{S_X(l, p)}{O(l, p)} \quad (\text{eq. 1})$$

229 Where :

- 230 •  $S_X(l, p)$  is the number of occurrences of the presence of oil X detected on a pixel by image-  
231 interpretation,  
232 • X is the type of oil. It can be natural leaks (oil seepages), pollution by boats (~~oil spill ships~~  
233 ~~spills from ships~~) and pollution by platforms (oil spills from platforms),  
234 •  $(l, p)$  are the coordinates  $(l, p)$  of the current pixel representing the rows and columns of the image,  
235 •  $O(l, p)$  are the number of observations as they appear in the footprints of the processed images Envisat  
236 ASAR WSM,  
237 •  $P_X(l, p)$  is the normalized occurrence also called probability of oil presence at pixel  $(l, p)$ .

238 For each class X of oil slick among (e) “seepage”, (s) “spill from ship”, and (p) “spill from platform”, the generic definition given in  
239 (eq.1) becomes the ones given in (eq.2).

$$P_e(l, p) = \frac{S_e(l, p)}{O(l, p)}, P_s(l, p) = \frac{S_s(l, p)}{O(l, p)}, P_p(l, p) = \frac{S_p(l, p)}{O(l, p)} \quad (\text{eq. 2})$$

240 Where :

- 241 •  $S_e(l, p)$ ,  $S_s(l, p)$  et  $S_p(l, p)$  are the number of occurrences of oil presence detected on a pixel by image-interpretation  
242 of -natural leaks (oil seepages), - ~~pollution of boats~~ (oil spills from ships) and -pollution of  
243 platforms (oil spills from platforms) respectively,  
244 •  $(l, p)$  are the coordinates  $(l, p)$  of the current pixel representing the rows and columns of the image,  
245 •  $O(l, p)$  are the number of observation as they appear in the footprints of the processed images Envisat  
246 ASAR WSM,

247 The total probability of presence of oil X per pixel  $(P_X(l, p))$  is equal to:

$$P_X(l, p) = \frac{S_e(l, p)}{O(l, p)} + \frac{S_s(l, p)}{O(l, p)} + \frac{S_p(l, p)}{O(l, p)} \quad (\text{eq. 3})$$

248 Thus, we denote by  $\hat{A}_X$  the mean area covered in oil of origin X in the Gulf of Guinea between 2002 and 2012. This mean area is given  
249 by (eq.4).

$$A_X = \sum_{GG}^l \sum_{GG}^p (P_X(l, p) \times A(l, p)) \approx \sum_{GG}^l \sum_{GG}^p (P_X(l, p)) \times \bar{A} \quad (\text{eq. 4})$$

250 Where:

- 251 •  $A(l, p)$  is the area of the pixel  $(l, p)$ ,  
252 •  $\bar{A}$  is the mean area of a pixel. Due to the chosen geographic coordinate reference system (CRS),  
253 the variation of the area of the pixel (75 m x 75 m) is less than 2.5 % over the Gulf of Guinea  
254 (GG).

255 For a given year Y, the mean area covered in oil of origin X ( $\hat{A}_{X,Y}$ ) is given by (eq.5).

$$A_{X,Y} = \sum_{GG}^I \sum_{GG}^P (P_{X,Y}(l, p)) \times \bar{A} \quad (\text{eq. 5})$$

256 Where:

257 •  $P_{X,Y}(l,p)$  is the probability of presence of oil of origin X for a given year Y for a given pixel (l,p).

258 For a given year Y and for a given EEZ, the mean area covered in oil of origin X ( $\hat{A}_{X,Y,EEZ}$ ) is given by (eq.6).

$$A_{X,Y,EEZ} = \sum_{EEZ}^I \sum_{EEZ}^P (P_{X,Y}(l, p)) \times \bar{A} \quad (\text{eq. 6})$$

#### 259 4.5. Mean fraction covered by oil for a given EEZ

260 For each country's EEZ over a given period of time, we estimated the mean fraction covered in oil of origin X and for a given year Y

261 ( $P_{X,Y,EEZ}$ ) by dividing the mean area covered in oil of origin X for a given year Y for a given EEZ ( $\hat{A}_{X,Y,EEZ}$ ) by the area of the country's

262 EEZ  $A_{EEZ}$  (eq.7). When presenting the results, the term EEZ was replaced by the country's ISO code.

$$P_{X,Y,EEZ} = \frac{A_{X,Y,EEZ}}{A_{EEZ}} \quad (\text{eq. 7})$$

---

## 263 5. Results and discussion

### 264 5.1. Spatial distribution of oil slicks in the Gulf of Guinea

265 The spatial and temporal analysis on the Gulf of Guinea allowed the image-interpretation of 18,063 oil slicks. The database of the 18,063  
266 identified objects includes two classes of mineral oil. On the one hand, anthropogenic pollution that come from oil spill platforms and  
267 recurring deballasting of oil spills from ships. On the other hand, natural oil seepage resurgences which are hints of the presence of  
268 hydrocarbon reservoirs in the sub-surface of the Gulf of Guinea.

269 The fig. 11 illustrates the spatial distribution of the 18,063 oil slicks that have been detected and then mapped in the Gulf of Guinea over  
270 the period 2002-2012. For each of the N slicks, a point has been designated as the source, forming a discrete dot map. In order to obtain a  
271 continuous density map, each source point of this dot map has been convoluted by a 2-D kernel function. In fact, the density map is the sum  
272 of each of these N kernel functions The fig. 12, fig. 13, and fig. 14 respectively show the density maps of oil seepages, spills s from ships and  
273 spill from platforms. The kernel function that has been used is:

$$K(r) = (1 - (r/0.7)^2)^2 \text{ if } r \leq 0.7 \quad (\text{eq. 8})$$

$$K(r) = 0 \text{ if } r > 0.7$$

274 Where r is the Euclidian distance to the source point in degrees.

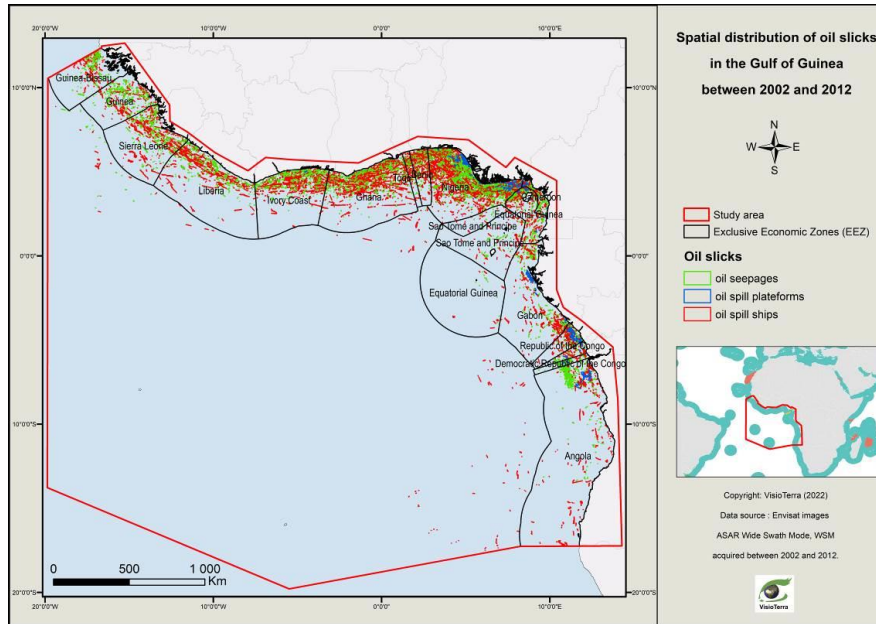


*fig. 11 - Spatial distribution of oil slicks in the Gulf of Guinea between 2002 and 2012.*

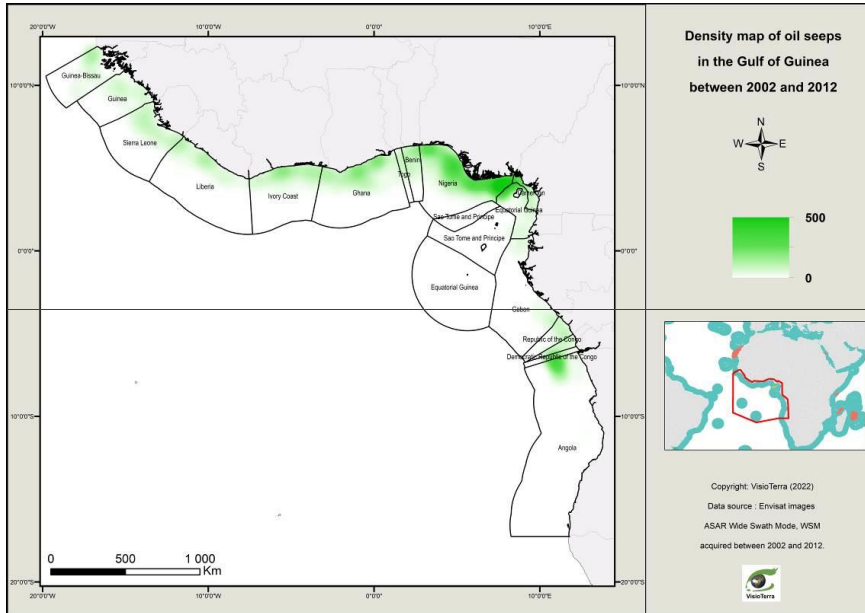
275

276

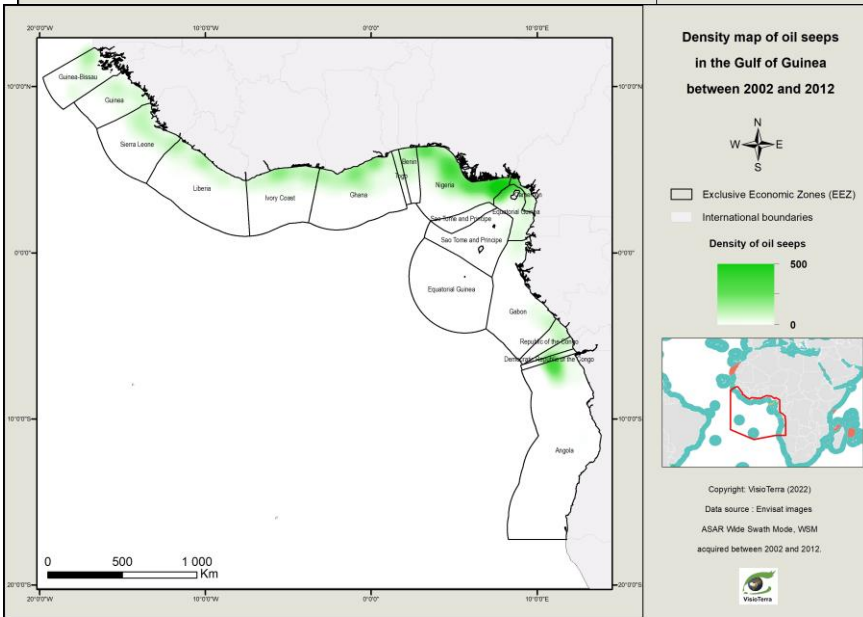
277 The fig. 12 shows that oil seepages are distributed over all the EEZs in the Gulf of Guinea. This large amount of oil seepages from the  
 278 Gulf of Guinea could be partly explained by its geology resulting from the opening of the South Atlantic domain initiated in the Lower  
 279 Cretaceous and by the significant sediment supply from the Niger Delta (Grimaud et al., 2018).

280 The proximity of the main maritime routes to the coasts contributes to the concentration of discharges in these places. This phenomenon  
 281 is especially noticed along the coasts of Nigeria which is one of the main shipping routes and occupies a place in maritime piracy (see  
 282 fig. 13). Thus, there are significant spills of ships there, despite the international convention for the prevention of pollution from ships  
 283 (MARPOL 73/78), which came into force in 1983. Illegal dumping operations include deballasting and cleaning of ship tanks.

284 Offshore oil platforms have been found all along the coasts of the EEZs of the top oil producing countries (Nigeria, Angola, Republic of  
 285 Congo, Ghana...) in the Gulf of Guinea (see fig. 14). The oil spills coming from platforms that have been observed in our study are very well  
 286 correlated with offshore installations.



287

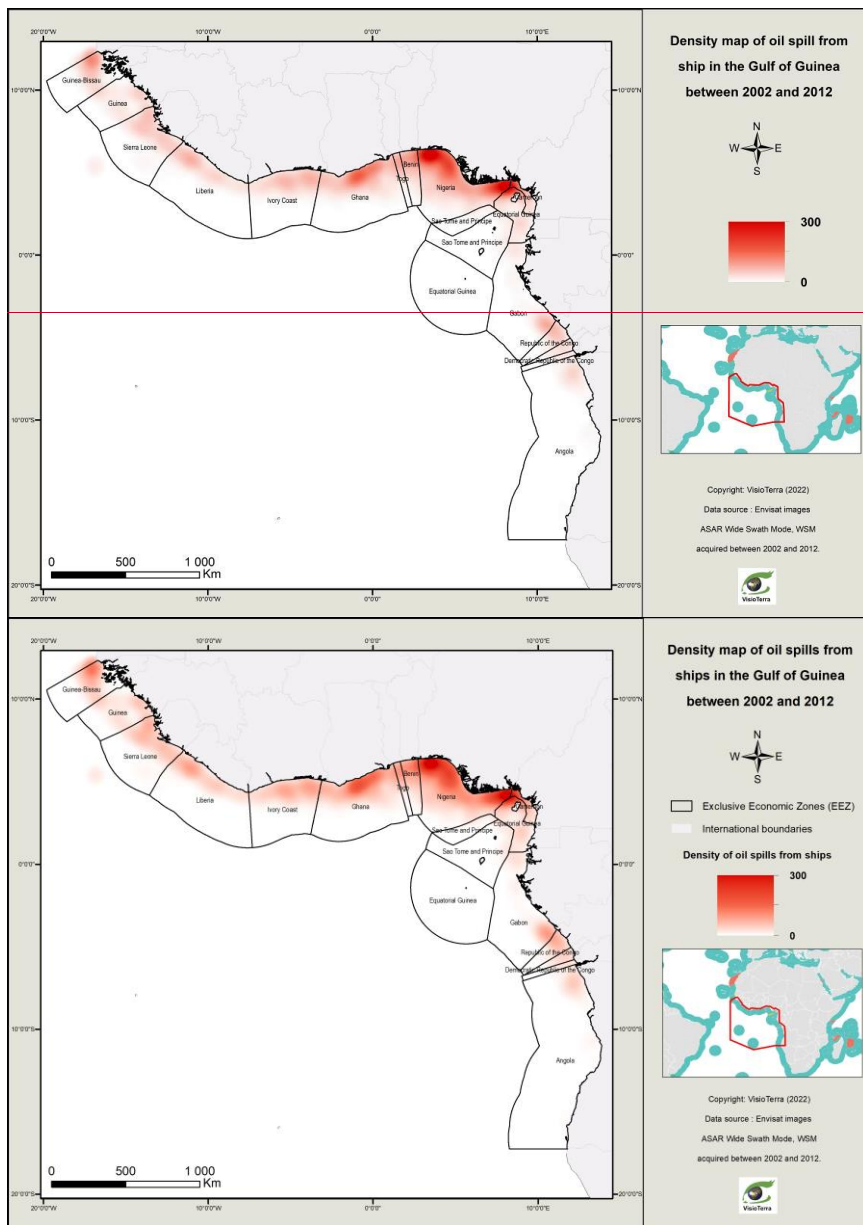


288

289

290

fig. 12 - Density map of oil seeps in the Gulf of Guinea between 2002 and 2012.



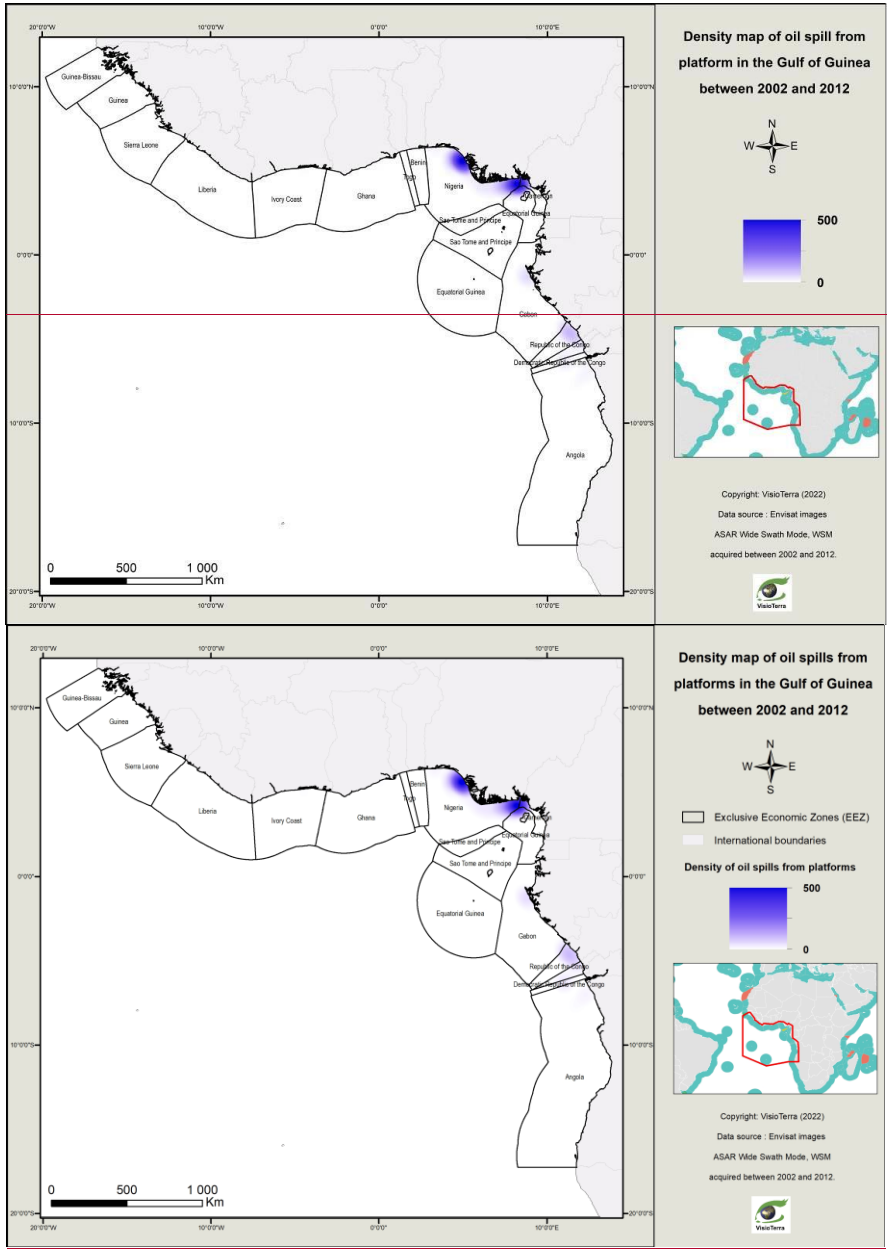
291

292

293

294

fig-12fig. 13 - Density map of oil spills from ships in the Gulf of Guinea between 2002 and 2012.



295

296

297

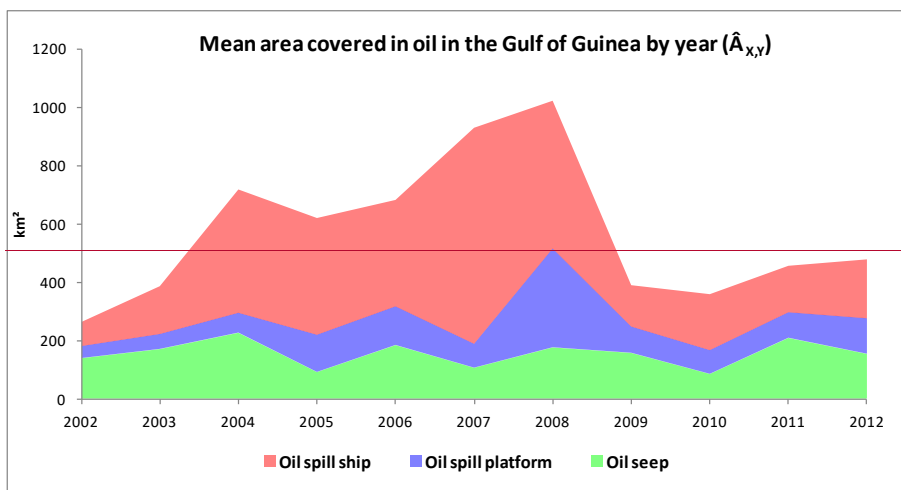
fig. 13 fig. 14 - Density map of oil spills from platforms in the Gulf of Guinea between 2002 and 2012.

298 **5.2. Mean area covered in oil ( $\hat{A}_{X,Y,EEZ}$ )**299 **5.2.1. Mean area covered in oil in the Gulf of Guinea ( $\hat{A}_{X,Y}$ )**

300 The fig. 15 shows the mean area covered in oil in the Gulf of Guinea by year. One may notice that:

- 301
- the mean area covered in oil slicks from natural origin (oil seeps) remains more or less stable during the period 2002-302 2012,
  - the mean area covered with oil slicks from oil spill platforms seems to have increased significantly during 2008 and303 then returned to normal in 2009 until the end of the study period,
  - the mean area covered in oil slicks from ships seems to have increased after 2004 with a peak between 2007 and 2008,304 then have fallen in 2009 and remained stable until the end of the study period.
- 305
- 306

307 The mean area covered with oil slicks over the entire Gulf of Guinea (GG) between 2002 and 2012 is 145 km<sup>2</sup> for oil seeps, 111 km<sup>2</sup> for308 oil spills from platform and 308 km<sup>2</sup> oil spills from ship and 547 km<sup>2</sup> for all oil slicks (table 1). That means that we have detected an oil slick309 area of 574 km<sup>2</sup> for a per “full-coverage observation” during 2002-2012. This result is very similar to the one obtained by Dong et al. (2022)310 that detects an oil slick area of 568 km<sup>2</sup> for a per “full-coverage observation” during 2014-2019 using Sentinel-1 data.



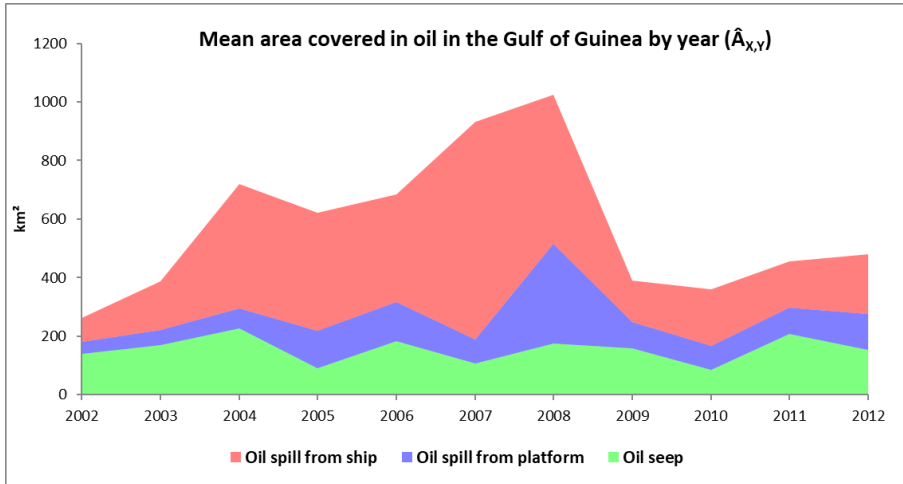


fig. 14 fig. 15 - Mean area covered in oil in the Gulf of Guinea by year ( $\hat{A}_{x,y}$ ).

Oil slicks	Mean area covered in oil in GG
Oil seep	154 km <sup>2</sup>
Oil spill from platform	111 km <sup>2</sup>
Oil spill from ship	308 km <sup>2</sup>
<b>Total</b>	<b>574 km<sup>2</sup></b>

table 1 – Temporal mean of the yearly mean area covered in oil in the Gulf of Guinea between 2002 and 2012.

#### 5.2.2. Mean area covered in oil by EEZ of country ( $\hat{A}_{x,y,EEZ}$ )

The fig. 16 shows the mean area covered in oil by EEZ of countries between 2002 and 2012. The fig. 17 shows the mean area covered in oil by EEZ of countries by year. One may notice that the most polluted EEZ are Nigeria followed by Angola, Republic of Congo and Cameroon.

The analysis by EEZ shows that the decrease in oil spills observed between 2008 and 2009 (fig. 15) was driven by the major oil producing countries: Angola, Nigeria and Republic of Congo (fig. 17).

The fall in the mean area covered in oil from platforms and ships may be explained by the economic crisis of 2008. In fact, 2008 world crisis had led to the falling in oil prices inducing deficit in the budget of oil companies and governments. For instance, Angola oil production decreased in 2009 following the post-2008 slowdown in global economic activity and the subsequent glut of oil on the global market (Mikidadu, 2018).

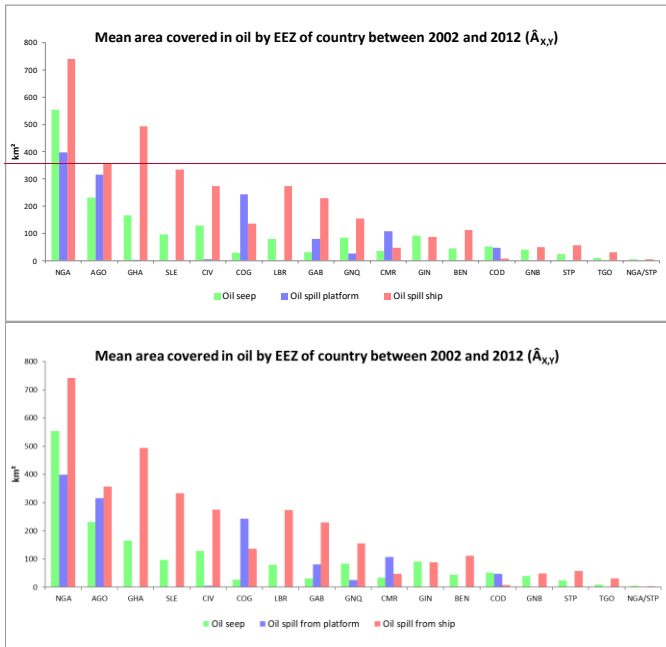
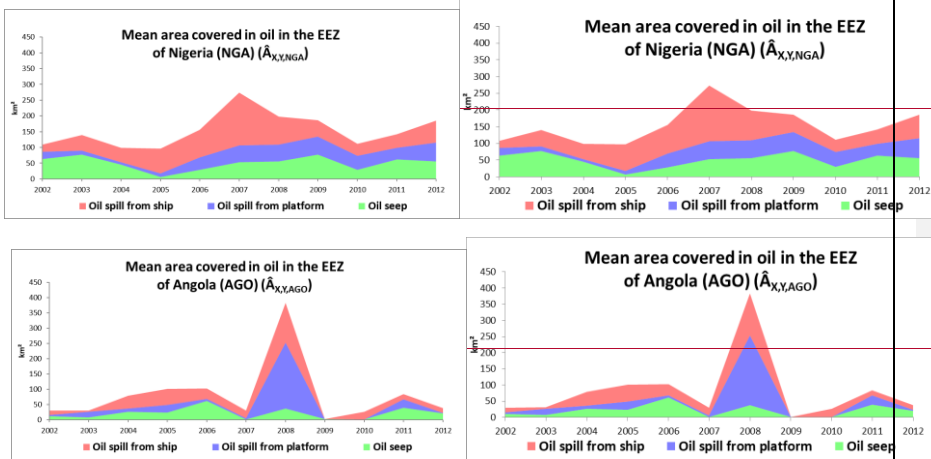


fig. 15 fig. 16 - Mean area covered in oil by EEZ of country ( $\hat{A}_{x,y}$ ) between 2002 and 2012.



325

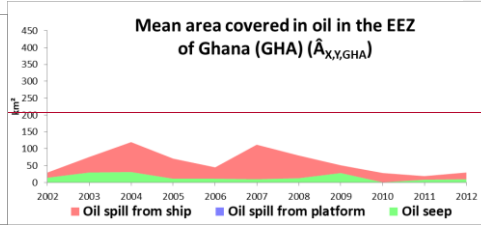
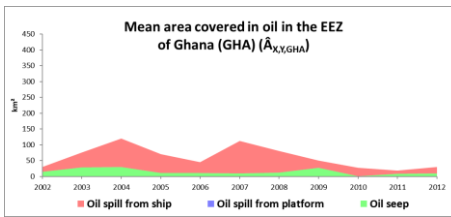
326

327

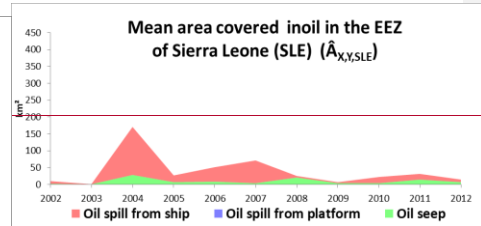
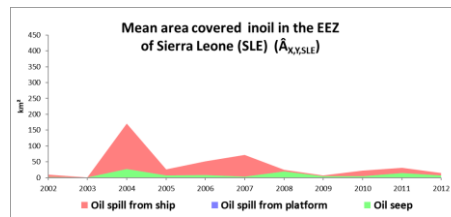
328

329

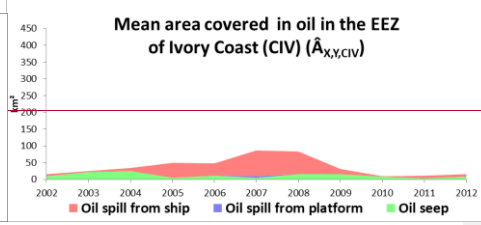
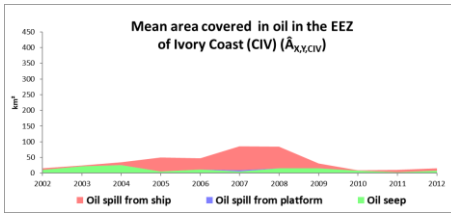
330



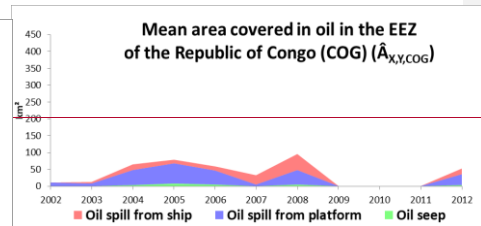
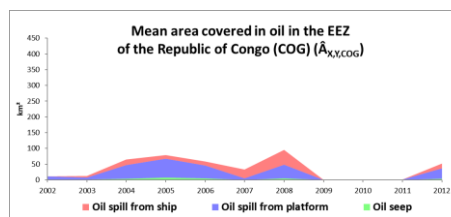
331



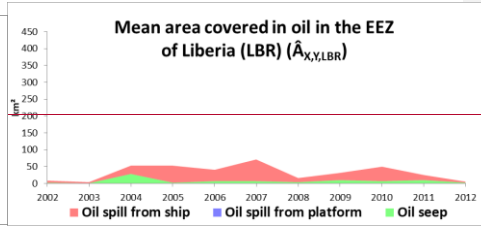
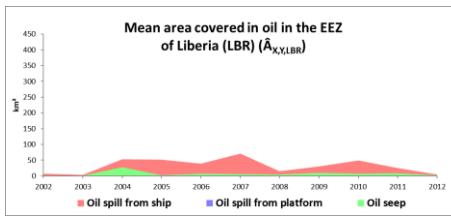
332



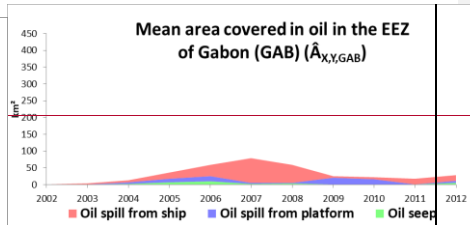
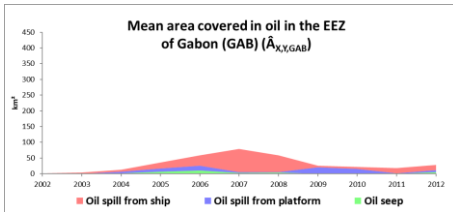
333



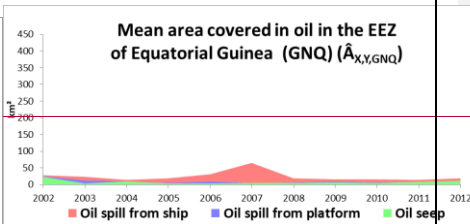
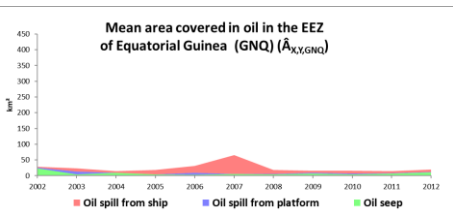
334



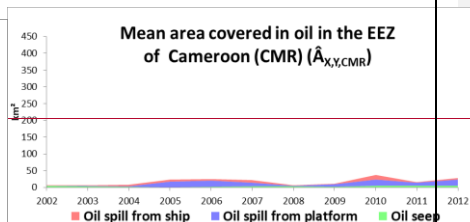
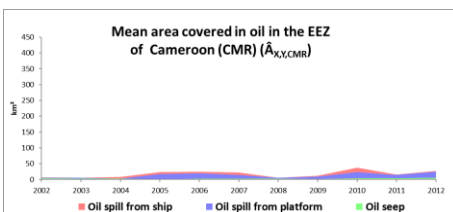
335



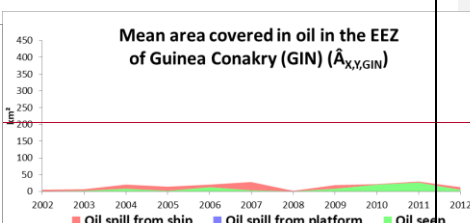
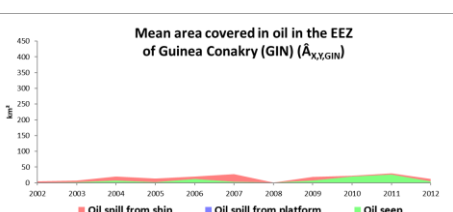
336



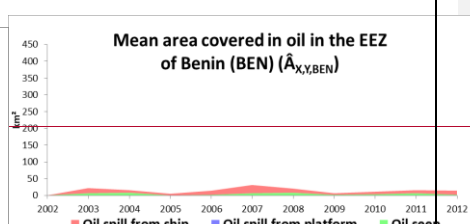
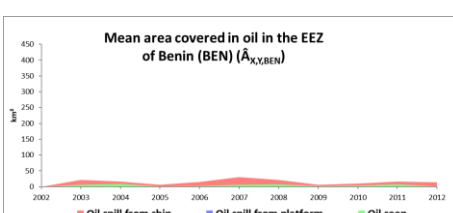
337



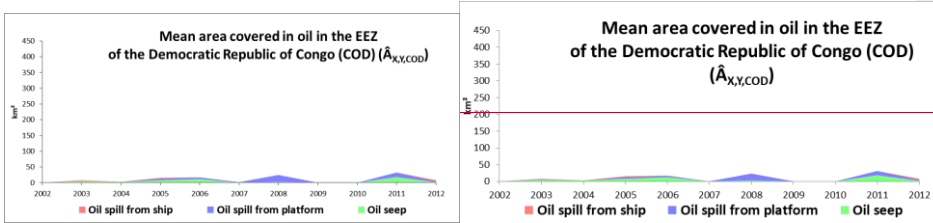
338



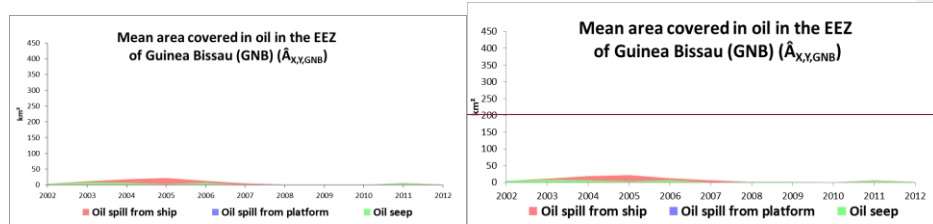
339



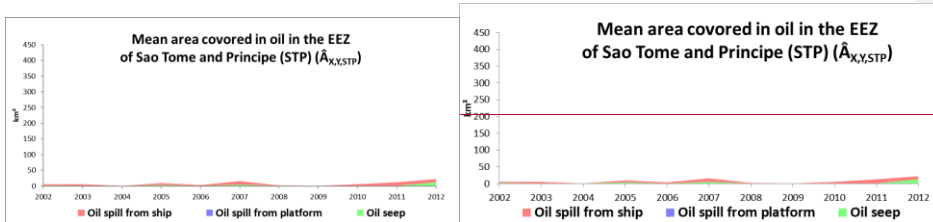
340



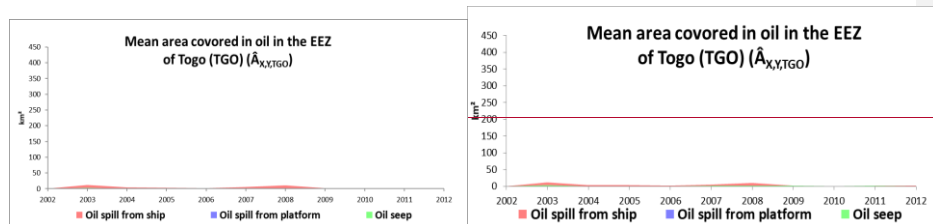
341



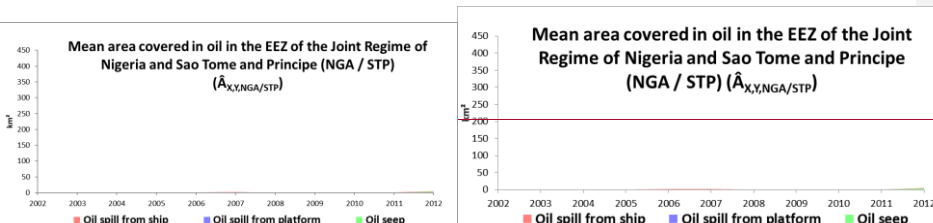
342



343



344



345

fig. 16 fig. 17 - Mean area covered in oil by EEZ of countries per year ( $\hat{A}_{X,Y,EEZ}$ ).

346

5.3. Mean fraction covered by oil by EEZ ( $P_{X,Y,EEZ}$ )

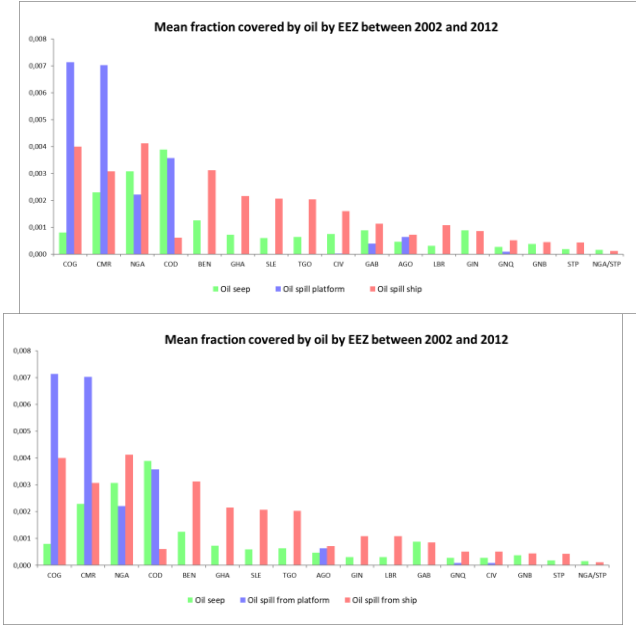
347

As shown in fig.15, Nigeria holds the record for pollution by platforms and also by boats. These data incorporated the pollution observed

348 throughout its whole EEZ. But isn't it also because Nigeria has an extended EEZ? To make the analysis independent of the size of the EEZ,  
 349 we calculate the "Mean fraction covered by oil by EEZ".

350 The fig. 18 shows the mean fraction covered by oil by EEZ of countries between 2002 and 2012. The fig. 19 shows the mean fraction  
 351 covered by oil by EEZ of countries by year.

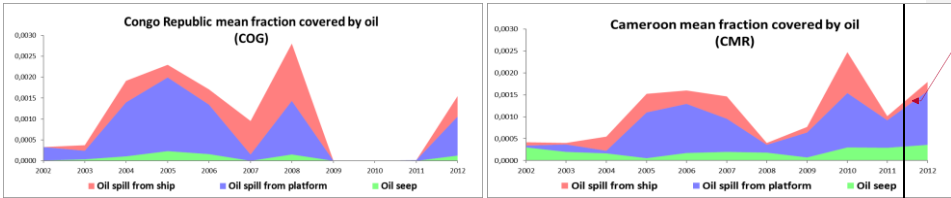
352 The country mean fraction covered by oil which divides the mean area covered in oil by the country EEZ area (eq.7) gives an idea of the  
 353 mean probability to be covered by oil by EEZ. Thus, the largest the mean fraction is, the more the area is likely to be covered by it. One may  
 354 see that the probability that an oil spill occurs is high for the Republic of Congo, Cameroon and Nigeria while the probability that an oil seep  
 355 occurs is high for the Democratic Republic of the Congo, Nigeria and Cameroon.



356

357

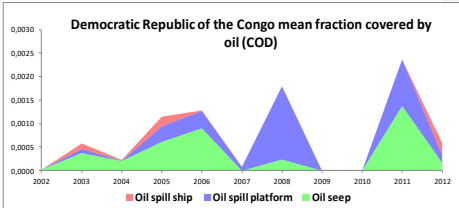
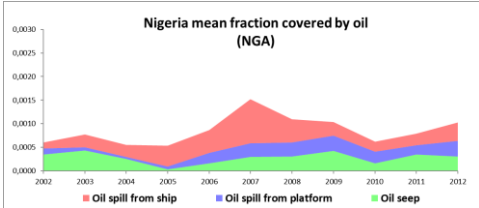
358 *fig. 17 fig. 18 - Mean fraction covered by spilled oil by EEZ between 2002 and 2012.*



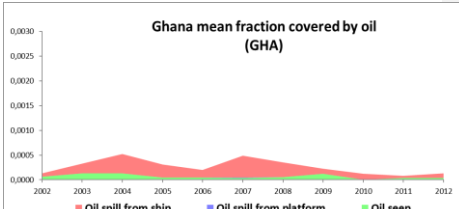
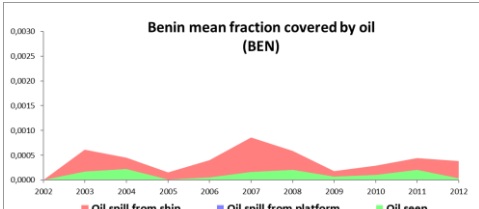
359

Mis en forme : Interligne : 1,5 ligne

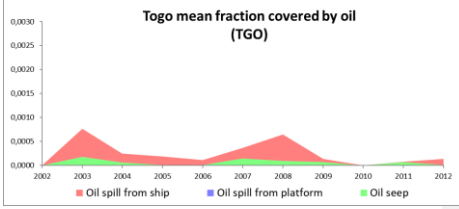
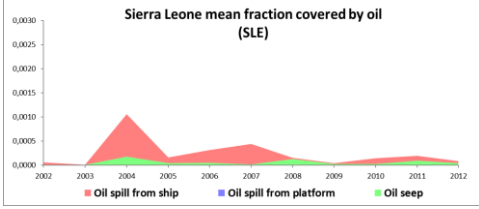
360



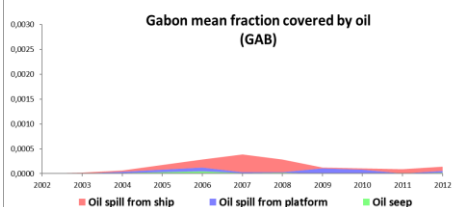
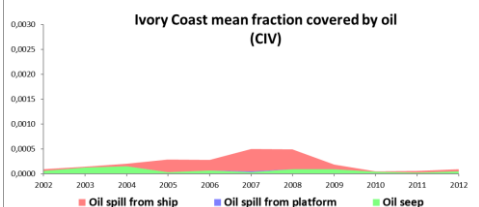
361



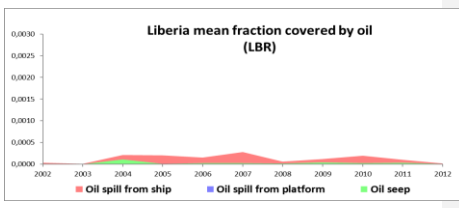
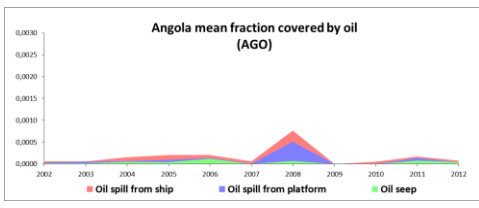
362



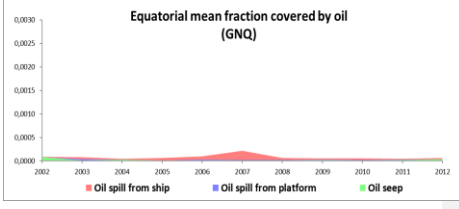
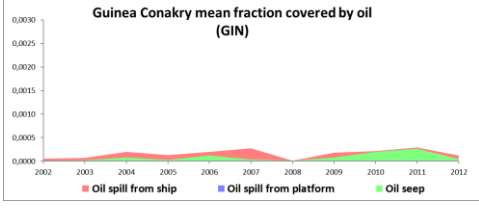
363



364



365



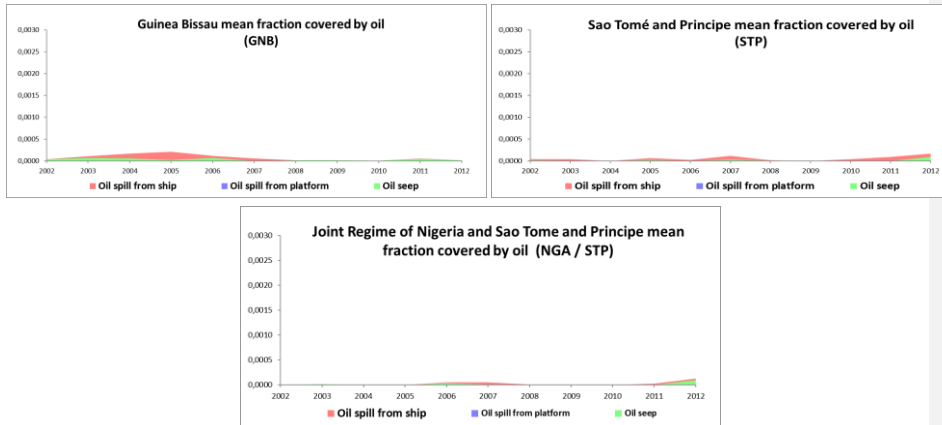


Fig. 19 - Mean fraction covered by oil by EEZ by year.

## 6. Data availability

All the Envisat ASAR images (2002-2012) used in this study are available at ESA website <https://eocat.esa.int/sec/#data-services-area>. These data can also be viewed on the HEDAVI (Heritage Data Visualization) portal managed by VisioTerra at the address <http://hedavi.esa.int/>. The spatial distribution of the oil slicks in the Gulf of Guinea between 2002 and 2012 is available at ZENODO: <https://doi.org/10.5281/zenodo.6470470> (Najoui, 2022).

A set of 100 georeferenced oil spills is available at ZENODO: <https://doi.org/10.5281/zenodo.6907743> (Najoui, 2022).

## 7. Conclusion and perspectives

An unprecedented database of oil spills has been generated over the EEZ of the Gulf of Guinea using the 11 years of acquisitions of SAR images at C-band by ASAR in wide-swath mode (150 m of spatial resolution) contained in the archive of the Envisat mission. This database has been achieved using a manual approach. The present study shows that all of the countries EEZ are sites of natural oil seepages due to the extensive geological context of the Gulf of Guinea. It shows also that oil spills from ships are well correlated to the shipping routes along the coasts of the 17 EEZ of the Gulf of Guinea while oil spills coming from oil platforms are concentrated along the coasts of oil-producing countries like Nigeria, Republic of Congo, Angola, and Ghana. The temporal analysis during 10 years (2002-2012) shows a decrease in the mean area covered by oil between 2008 and 2009. This decrease is likely to be due to the post-2008 global economic slowdown.

Oil seepages and oil spills monitoring will benefit from Sentinel-1 mission, launched in 2014, owing to its higher spatial resolution (10 m), its temporal resolution (6 days), and its longer period of acquisitions (beyond 2032). This dataset will offer more reliable and timely information for emergency and mitigation policies.

### Acknowledgments

The authors would like to thank the ESA (European Spatial Agency) for providing the SAR scenes used in this study.

- 389 Adelana, S., Adeosun, T., 2011. Environmental pollution and remediation: challenges and management of oil Spillage in the Nigerian coastal  
390 areas. *Am. J. Sci. Ind. Res.* 2, 834–845. <https://doi.org/10.5251/ajsir.2011.2.6.834.845>
- 391 Albakjaji, M., 2010. La pollution de la mer méditerranée par les hydrocarbures liée au trafic maritime.
- 392 Alpers, W., Holt, B., Zeng, K., 2017. Oil spill detection by imaging radars: Challenges and pitfalls. *Remote Sens. Environ.* 201, 133–147.  
393 <https://doi.org/10.1016/j.rse.2017.09.002>
- 394 Bagby, S.C., Reddy, C.M., Aepli, C., Fisher, G.B., Valentine, D.L., 2017. Persistence and biodegradation of oil at the ocean floor following  
395 *Deepwater Horizon*. *Proc. Natl. Acad. Sci.* 114, E9–E18. <https://doi.org/10.1073/pnas.1610110114>
- 396 Brekke, C., Solberg, A.H.S., 2008. Classifiers and Confidence Estimation for Oil Spill Detection in ENVISAT ASAR Images. *IEEE Geosci.*  
397 *Remote Sens. Lett.* 5, 65–69. <https://doi.org/10.1109/LGRS.2007.907174>
- 398 Brekke, C., Solberg, A.H.S., 2005. Oil spill detection by satellite remote sensing. *Remote Sens. Environ.* 95, 1–13.  
399 <https://doi.org/10.1016/j.rse.2004.11.015>
- 400 Caruso, M., Migliaccio, M., Hargrove, J., Garcia-Pineda, O., Graber, H., 2013. Oil Spills and Slicks Imaged by Synthetic Aperture Radar.  
401 *Oceanography* 26. <https://doi.org/10.5670/oceanog.2013.34>
- 402 Chalghmi, H., 2015. Etude de la pollution marine par les hydrocarbures et caractérisation de leurs effets biochimiques et moléculaires sur la  
403 palourde de *Ruditapes* sp.
- 404 Del Frate, F., Petrocchi, A., Lichtenegger, J., Calabresi, G., 2000. Neural networks for oil spill detection using ERS-SAR data. *IEEE Trans.*  
405 *Geosci. Remote Sens.* 38, 2282–2287. <https://doi.org/10.1109/36.868885>
- 406 Dong, Y., Liu, Y., Hu, C., MacDonald, I.R., Lu, Y., 2022. Chronic oiling in global oceans. *Science* 376, 1300–1304.  
407 <https://doi.org/10.1126/science.abm5940>
- 408 Espedal, H.A., 1999. Satellite SAR oil spill detection using wind history information. *Int. J. Remote Sens.* 20, 49–65.  
409 <https://doi.org/10.1080/014311699213596>
- 410 Favennec, J.-P., Copinchi, P., Cavatorta, T., Esen, F., 2003. Les nouveaux enjeux pétroliers en Afrique. *Polit. Afr.* 89, 127.  
411 <https://doi.org/10.3917/polaf.089.0127>
- 412 Fingas, M., Brown, C., 2017. A Review of Oil Spill Remote Sensing. *Sensors* 18, 91. <https://doi.org/10.3390/s18010091>
- 413 Fiscella, B., Giancaspro, A., Nirchio, F., Pavese, P., Trivero, P., 2000. Oil spill detection using marine SAR images. *Int. J. Remote Sens.* 21,  
414 3561–3566. <https://doi.org/10.1080/014311600750037589>
- 415 Fuhrer, M., 2012. Transport maritime de produits chimiques liquides et flottants : étude expérimentale du rejet accidentel sous-marin suite a  
416 un naufrage.
- 417 Gade, M., Alpers, W., Hühnerfuss, H., Masuko, H., Kobayashi, T., 1998. Imaging of biogenic and anthropogenic ocean surface films by the  
418 multifrequency/multipolarization SIR-C/X-SAR. *J. Geophys. Res. Oceans* 103, 18851–18866. <https://doi.org/10.1029/97JC01915>
- 419 Garcia-Pineda, O., MacDonald, I., Zimmer, B., 2008. Synthetic Aperture Radar Image Processing using the Supervised Textural-Neural  
420 Network Classification Algorithm, in: IGARSS 2008 - 2008 IEEE International Geoscience and Remote Sensing Symposium.  
421 *IEEE, Boston, MA, USA*, p. IV-1265-IV-1268. <https://doi.org/10.1109/IGARSS.2008.4779960>
- 422 Grimaud, J.-L., Rouby, D., Chardon, D., Beauvais, A., 2018. Cenozoic sediment budget of West Africa and the Niger delta. *Basin Res.* 30,  
423 169–186. <https://doi.org/10.1111/bre.12248>
- 424 Jackson, C.R., Apel, J.R., United States (Eds.), 2004. Synthetic aperture radar: marine user's manual. U.S. Dept. of Commerce : National  
425 Oceanic and Atmospheric Administration, Washington, D.C.
- 426 Jafarzadeh, H., Mahdianpari, M., Homayouni, S., Mohammadimanesh, F., Dabboor, M., 2021. Oil spill detection from Synthetic Aperture  
427 Radar Earth observations: a meta-analysis and comprehensive review. *GIScience Remote Sens.* 58, 1022–1051.  
428 <https://doi.org/10.1080/15481603.2021.1952542>
- 429 Jatiault, R., Dhont, D., Loncke, L., Dubucq, D., 2017. Monitoring of natural oil seepage in the Lower Congo Basin using SAR observations.  
430 *Remote Sens. Environ.* 191, 258–272. <https://doi.org/10.1016/j.rse.2017.01.031>
- 431 Johannessen, O.M., Sandven, S., Jenkins, A.D., Durand, D., Pettersson, L.H., Espedal, H., Evensen, G., Hamre, T., 2000. Satellite earth  
432 observation in operational oceanography. *Coast. Eng.* 41, 155–176. [https://doi.org/10.1016/S0378-3839\(00\)00030-2](https://doi.org/10.1016/S0378-3839(00)00030-2)
- 433 Kanaa, T.F.N., Tonye, E., Mercier, G., Onana, V.P., Ngono, J.M., Frison, P.L., Rudant, J.P., Garello, R., 2003. Detection of oil slick  
434 signatures in SAR images by fusion of hysteresis thresholding responses, in: IGARSS 2003. 2003 IEEE International Geoscience  
435 and Remote Sensing Symposium. Proceedings (IEEE Cat. No.03CH37477). IEEE, Toulouse, France, pp. 2750–2752.  
436 <https://doi.org/10.1109/IGARSS.2003.1294573>
- 437 Khanna, S., Santos, M., Ustin, S., Shapiro, K., Haverkamp, P., Lay, M., 2018. Comparing the Potential of Multispectral and Hyperspectral  
438 Data for Monitoring Oil Spill Impact. *Sensors* 18, 558. <https://doi.org/10.3390/s18020558>
- 439 Kubat, M., Holte, R.C., Matwin, S., 1998. Machine Learning for the Detection of Oil Spills in Satellite Radar Images. *Mach. Learn.* 30, 195–  
440 215. <https://doi.org/10.1023/A:1007452223027>
- 441 Langangen, Ø., Olsen, E., Stige, L.C., Ohlberger, J., Yragina, N.A., Vikebø, F.B., Bogstad, B., Stenseth, N.C., Hjermmann, D.Ø., 2017. The

Mis en forme : Police :8 pt

Mis en forme : Police :8 pt, Français (France)

Mis en forme : Police :8 pt

Mis en forme : Police :8 pt, Français (France)

Mis en forme : Police :8 pt

Mis en forme : Police :8 pt, Français (France)

Mis en forme : Police :8 pt

Mis en forme : Police :8 pt, Français (France)

Mis en forme : Police :8 pt

Mis en forme : Police :8 pt, Français (France)

Mis en forme : Police :8 pt

Mis en forme : Police :8 pt, Français (France)

Mis en forme : Police :8 pt

Mis en forme : Police :8 pt, Français (France)

Mis en forme : Police :8 pt

- 442 effects of oil spills on marine fish: Implications of spatial variation in natural mortality. *Mar. Pollut. Bull.* 119, 102–109.  
443 <https://doi.org/10.1016/j.marpolbul.2017.03.037>
- 444 Lawrence, S.R., Munday, S., Bray, R., 2002. Regional geology and geophysics of the eastern Gulf of Guinea (Niger Delta to Rio Muni).  
445 *Lead. Edge* 21, 1112–1117. <https://doi.org/10.1190/1.1523752>
- 446 Leifer, I., Lehr, W.J., Simecek-Beatty, D., Bradley, E., Clark, R., Dennison, P., Hu, Y., Matheson, S., Jones, C.E., Holt, B., Reif, M.,  
447 Roberts, D.A., Svejckovsky, J., Swayze, G., Wozenraft, J., 2012. State of the art satellite and airborne marine oil spill remote  
448 sensing: Application to the BP Deepwater Horizon oil spill. *Remote Sens. Environ.* 124, 185–209.  
449 <https://doi.org/10.1016/j.rse.2012.03.024>
- 450 Li, Y., Hu, C., Quigg, A., Gao, H., 2019. Potential influence of the Deepwater Horizon oil spill on phytoplankton primary productivity in the  
451 northern Gulf of Mexico. *Environ. Res. Lett.* 14, 094018. <https://doi.org/10.1088/1748-9326/ab3735>
- 452 Li, Z., Johnson, W., 2019. An Improved Method to Estimate the Probability of Oil Spill Contact to Environmental Resources in the Gulf of  
453 Mexico. *J. Mar. Sci. Eng.* 7, 41. <https://doi.org/10.3390/jmse7020041>
- 454 Liu, A.K., Peng, C.Y., Chang, S.Y.-S., 1997. Wavelet analysis of satellite images for coastal watch. *IEEE J. Ocean. Eng.* 22, 9–17.  
455 <https://doi.org/10.1109/48.557535>
- 456 Louet, J., Bruzzi, S., 1999. ENVISAT mission and system. in: *IEEE 1999 International Geoscience and Remote Sensing Symposium.*  
457 *IGARSS'99 (Cat. No.99CH36293)*. Presented at the IEEE 1999 International Geoscience and Remote Sensing Symposium.  
458 *IGARSS'99, IEEE, Hamburg, Germany*, pp. 1680–1682. <https://doi.org/10.1109/IGARSS.1999.772059>
- 459 MacDonald, I.R., Garcia-Pineda, O., Beet, A., Daneshgar Asl, S., Feng, L., Graettinger, G., French-McCay, D., Holmes, J., Hu, C., Huffer,  
460 F., Leifer, I., Muller-Karger, F., Solow, A., Silva, M., Swayze, G., 2015. Natural and unnatural oil slicks in the Gulf of Mexico.  
461 *J. Geophys. Res. Oceans* 120, 8364–8380. <https://doi.org/10.1002/2015JC011062>
- 462 Marghany, M., 2015. Automatic detection of oil spills in the Gulf of Mexico from RADARSAT-2 SAR satellite data. *Environ. Earth Sci.* 74,  
463 5935–5947. <https://doi.org/10.1007/s12665-015-4617-y>
- 464 Mercier, G., Girard-Arduin, F., 2006. Partially Supervised Oil-Slick Detection by SAR Imagery Using Kernel Expansion. *IEEE Trans.*  
465 *Geosci. Remote Sens.* 44, 2839–2846. <https://doi.org/10.1109/TGRS.2006.881078>
- 466 Mfewou, A., Tchekote, H., Lemougue, J., 2018. Frontières Et Dynamiques Socio-Spatiales En Afrique: Une Analyse À Partir Des  
467 Frontières Sud- Camerounaises. *Eur. Sci. J. ESJ* 14, 285. <https://doi.org/10.19044/esj.2018.v14n5p285>
- 468 Mikidadu, M., 2018. Oil Production and Economic Growth in Angola. *Int. J. Energy Econ. Policy* 8, 127–131.
- 469 Miranda, N., Rosich, B., Meadows, P.J., Haria, K., Small, D., Schubert, A., Lavalle, M., Collard, F., Johnsen, H., Monti-Guarnieri, A.,  
470 D'Aria, D., 2013. The Envisat ASAR mission: A look back at 10 years of operation. <https://doi.org/10.5167/UZH-96146>
- 471 NAE-NRC, 2012. Macondo Well Deepwater Horizon Blowout: Lessons for Improving Offshore Drilling Safety. National Academies Press,  
472 Washington, D.C. <https://doi.org/10.17226/13273>
- 473 Najoui, Z., 2022. Spatial distribution of oil slicks in the Gulf of Guinea between 2002 and 2012. *Zenodo*.  
474 <https://doi.org/10.5281/ZENODO.6470470>
- 475 Najoui, Z., 2022. 100 geolocated oil spills in the Gulf of Guinea. <https://doi.org/10.5281/ZENODO.6907743>
- 476 Najoui, Z., 2017. Prétraitement optimal des images radar et modélisation des dérives de nappes d'hydrocarbures pour l'aide à la photo-  
477 interprétation en exploration pétrolière et surveillance environnementale.
- 478 Najoui, Z., Riazanoff, S., Deffontaines, B., Xavier, J.-P., 2018a. Estimated location of the seafloor sources of marine natural oil seeps from  
479 sea surface outbreaks: A new "source path procedure" applied to the northern Gulf of Mexico. *Mar. Pet. Geol.* 91, 190–201.  
480 <https://doi.org/10.1016/j.marpetgeo.2017.12.035>
- 481 Najoui, Z., Riazanoff, S., Deffontaines, B., Xavier, J.-P., 2018b. A Statistical Approach to Preprocess and Enhance C-Band SAR Images in  
482 Order to Detect Automatically Marine Oil Slicks. *IEEE Trans. Geosci. Remote Sens.* 56, 2554–2564.  
483 <https://doi.org/10.1109/TGRS.2017.2760516>
- 484 Ngodi, E., 2005. Gestion des ressources pétrolières et développement en Afrique.
- 485 Okafor-Yarwood, I., 2018. The effects of oil pollution on the marine environment in the Gulf of Guinea—the Bonga Oil Field example.  
486 *Transnatl. Leg. Theory* 9, 254–271. <https://doi.org/10.1080/20414005.2018.1562287>
- 487 Ovardia, J.S., 2016. The petro-developmental state in Africa: making oil work in Angola, Nigeria and the Gulf of Guinea. Hurst & Company,  
488 London.
- 489 Pinkston, F.W.M., Flemings, P.B., 2019. Overpressure at the Macondo Well and its impact on the Deepwater Horizon blowout. *Sci. Rep.* 9,  
490 7047. <https://doi.org/10.1038/s41598-019-42496-0>
- 491 Reuscher, M.G., Baguley, J.G., Montagna, P.A., 2020. The expanded footprint of the Deepwater Horizon oil spill in the Gulf of Mexico  
492 deep-sea benthos. *PLOS ONE* 15, e0235167. <https://doi.org/10.1371/journal.pone.0235167>
- 493 Scheren, P.A., Ibe, A.C., Janssen, F.J., Lemmens, A.M., 2002. Environmental pollution in the Gulf of Guinea – a regional approach. *Mar.*  
494 *Pollut. Bull.* 44, 633–641. [https://doi.org/10.1016/S0025-326X\(01\)00305-8](https://doi.org/10.1016/S0025-326X(01)00305-8)
- 495 Shu, Y., Li, J., Yousif, H., Gomes, G., 2010. Dark-spot detection from SAR intensity imagery with spatial density thresholding for oil-spill  
496 monitoring. *Remote Sens. Environ.* 114, 2026–2035. <https://doi.org/10.1016/j.rse.2010.04.009>

Mis en forme : Police :8 pt, Français (France)

Mis en forme : Police :8 pt

Mis en forme : Police :8 pt, Français (France)

Mis en forme : Police :8 pt

Mis en forme : Police :8 pt, Français (France)

Mis en forme : Police :8 pt

Mis en forme : Police :8 pt, Français (France)

Mis en forme : Police :8 pt

Mis en forme : Police :8 pt, Français (France)

Mis en forme : Police :8 pt

- 497 Solberg, A.H.S., Storvik, G., Solberg, R., Volden, E., 1999. Automatic detection of oil spills in ERS SAR images. *IEEE Trans. Geosci.*  
498 *Remote Sens.* 37, 1916–1924. <https://doi.org/10.1109/36.774704>
- 499 Suresh, G., Melsheimer, C., Korber, J.-H., Bohrmann, G., 2015. Automatic Estimation of Oil Seep Locations in Synthetic Aperture Radar  
500 Images. *IEEE Trans. Geosci. Remote Sens.* 53, 4218–4230. <https://doi.org/10.1109/TGRS.2015.2393375>
- 501 The ENVISAT Mission and System, n.d.
- 502 Trivero, P., Biamino, W., 2010. Observing Marine Pollution with Synthetic Aperture Radar, in: Imperatore, P., Riccio, D. (Eds.), *Geoscience*  
503 *and Remote Sensing New Achievements*. InTech. <https://doi.org/10.5772/9106>
- 504 Tull, D.M., 2008. *Oil and Politics in the Gulf of Guinea* by Ricardo Soares de Oliveira London: Hurst & Co/New York: Columbia University  
505 Press, 2007. Pp. 379. £20.00 (pb). *J. Mod. Afr. Stud.* 46, 692–694. <https://doi.org/10.1017/S0022278X08003558>
- 506 Xu, L., Shafiee, M.J., Wong, A., Li, F., Wang, L., Clausi, D., 2015. Oil spill candidate detection from SAR imagery using a thresholding-  
507 guided stochastic fully-connected conditional random field model, in: 2015 IEEE Conference on Computer Vision and Pattern  
508 Recognition Workshops (CVPRW). IEEE, Boston, MA, USA, pp. 79–86. <https://doi.org/10.1109/CVPRW.2015.7301386>
- 509 Yaghamour, F., Els, J., Maio, E., Whittington-Jones, B., Samara, F., El Sayed, Y., Ploeg, R., Alzaabi, A., Philip, S., Budd, J., Mupandawana,  
510 M., 2022. Oil spill causes mass mortality of sea snakes in the Gulf of Oman. *Sci. Total Environ.* 825, 154072.  
511 <https://doi.org/10.1016/j.scitotenv.2022.154072>
- 512 Zhang, Y., Li, Y., Lin, H., 2014. *Oil-Spill Pollution Remote Sensing by Synthetic Aperture Radar*, in: Marghany, M. (Ed.), *Advanced*  
513 *Geoscience Remote Sensing*. InTech. <https://doi.org/10.5772/57477>

Mis en forme : Police :8 pt, Français (France)

Mis en forme : Police :8 pt